8A.1 The Relative Importance of Assimilating Radial Velocity and Reflectivity Data to Storm-Scale Analysis and Forecast

Jidong Gao[1*], Guoqing Ge[1,3], David J. Stensrud[2], and Ming Xue[1,3]

[1]Center for Analysis and Prediction of Storms, University of Oklahoma,

[2]National Severe Storm Laboratory/NOAA,

[3]School of Meteorology, University of Oklahoma, Norman, OK

1. Introduction

The NEXRAD (WSR-88D) Doppler radar network allows meteorologists to track severe weather events and provide better warning information to the public, ultimately saving lives and reducing property damage. However, the assimilation of such data into NWP models to provide physically consistent three-dimensional analyses and short-term forecasts has not been extensively explored. Since Doppler radar is the only operational instrument capable of providing observations of sufficient spatial and temporal resolution to capture convective-scale phenomena, the assimilation of reflectivity and velocity data from Doppler radars is vital to predicting ongoing convection and is part of the "warn on forecast" vision of the National Weather Service described in Stensrud et al. (2009).

Several methods exist for the assimilation of radar data. Sun et al (1991) and Sun and Crook (1997, 1998) have shown that four-dimensional variation analysis (4DVAR) is an idealized approach to assimilate radar data. However, To assimilate radar data, 4DVAR has so far been limited to relatively simple model configurations, usually with warm-rain microphysics only (Sun 2005). Computational cost and strong nonlinearity with model physics, including ice microphysics, often causes difficulties in 4DVAR assimilation of radar data. Ensemble Kalman filter (EnKF) is another advanced method for assimilating radar data (Snyder and Zhang 2003; Zhang et al. 2004; Dowell et al. 2004; Tong and Xue 2005; Gao and Xue 2008). Caya et al. (2005) showed that EnKF and 4DVAR produce analyses of generally similar quality and computational cost. Though these two methods are advanced methods theoretically, they are rather expensive computationally, especially at the convection-resolving resolution.

For realtime analysis and forecasting for convective weather, the three-dimensional (3DVAR)

* *corresponding author address*: Jidong Gao, [1]Center for Analysis and Prediction of Storms, University of Oklahoma, e-mail: jdgao@ou.edu

data assimilation method is a computationally efficient method comparing to 4DVAR and EnKF (Gao et al. 1999, Xiao et al. 2005). A 3DVAR system, ARPS 3DVAR system, is developed for ARPS model (Xue et al. 2000, 2001, and 2003). As described in Gao et al (2002; 2004), the ARPS 3DVAR system is capable of analyzing radar radial velocity data along with conventional observations in a very efficient way. To compensate the lack of a time dimension in 3DVAR method, experiments are usually performed using rapid intermittent analysis cycles to make better use of data distributed in time (Hu et al. 2006a, b). The ARPS 3DVAR system is usually supplemented by a cloud analysis package which analyzes hydrometer variables using radar reflectivity and satellite observations. Several studies (e.g. Hu et al. 2006a, b; Ge et al. 2009; Schenkman et al. 2009) have shown reasonable success in simulating and forecasting convective storms including tornadoes and supercells using the ARPS 3DVAR data assimilation system.

In this study, we seek to investigate the relative importance of assimilating radial velocity and reflectivity data to storm-scale analysis and forecast by using the 3DVAR and its cloud analysis system. The impact of assimilating radial velocity and/or reflectivity data from a WSR-88D network near central Oklahoma is examined using both an idealized case and a real data case. Hu et al. (2006a) showed that both radial wind and reflectivity data are very important for on-going storm development and forecasts. However, which type of radar data is more important has not been thoroughly examined for strong convective weather events.

This paper is organized as follows. Section 2 describes model parameters, and data assimilation method in detail. Section 3 provides configuration of the various experiments. Section 4 discusses the results of intermittent assimilation and forecasts cycles for an idealized case on a 1-km grid, and the results from the 400 Greensburg tornadic thunderstorm case is presented in section 5. Summary and conclusions are given in section 6.

2. The ARPS model, 3DVAR system and cloud analysis scheme

ARPS is used as the prediction model in this study. It is a general-purpose three-dimensional, non-hydrostatic and compressible atmospheric model which is well documented in several early publications (Xue et al. 2000, 2001 and 2003). In this section, we will only briefly review ARPS 3DVAR data assimilation system and cloud analysis scheme. Following Gao et al. (2004), the standard cost function of 3DVAR can be written as,

$$J(\mathbf{x}) = \frac{1}{2}\left(\mathbf{x}-\mathbf{x}^b\right)^T \mathbf{B}^{-1}\left(\mathbf{x}-\mathbf{x}^b\right) + \frac{1}{2}\left[H(\mathbf{x})-\mathbf{y}^o\right]^T \mathbf{R}^{-1}\left[H(\mathbf{x})-\mathbf{y}^o\right] + J_c(\mathbf{x}) \qquad (1)$$

where the first term on the right hand side measures the departure of the analysis vector, $\boldsymbol{x}$, from the background, $\boldsymbol{x}^b$, weighted by the inverse of the background error covariance matrix **B**. In the current

ARPS 3DVAR system, the analysis vector ***x*** contains the three wind components (*u*, *v*, and *w*), potential temperature (θ), pressure (*p*) and water vapor mixing ratio (q_v). The second, observation term, measures the departure of the analysis from the observation vector, $\mathbf{y}^o$. In this study, $\mathbf{y}^o$ only includes radar radial velocity data. The analysis is projected to the observation space by the forward operator *H* which is defined by forward radial wind equations and interpolation operator from model grid points to radar observation locations. The observation term is weighted by the inverse of observation error covariance matrix **R** that includes both the instrument and representativeness errors.

Term $J_c(\mathbf{x})$ in Eq. (1) represents dynamic or equation constraints. By defining $\sqrt{\mathbf{B}}\mathbf{v} = \left(\mathbf{x} - \mathbf{x}^b\right)$, the cost function is changed into incremental form:

$$J_{inc}(\mathbf{v}) = \frac{1}{2}\mathbf{v}^T\mathbf{v} + \frac{1}{2}\left(\mathbf{H}\mathbf{B}^{1/2}\mathbf{v} - \mathbf{d}\right)^T \mathbf{R}^{-1}\left(\mathbf{H}\mathbf{B}^{1/2}\mathbf{v} - \mathbf{d}\right) + J_c(\mathbf{v}) \quad (2)$$

where **H** is the linearized version of *H* and $\mathbf{d} \equiv \mathbf{y}^o - H\left(\mathbf{x}^b\right)$. In the current version of the ARPS 3DVAR system, the cross-correlations between variables are not included in the background error covariances. The spatial covariances for background error are modeled by a recursive filter (Purser, 2003a, 2003b). The corresponding covariance matrix, **R**, is diagonal, and its diagonal elements are specified according to the estimated observation errors.

In ARPS 3DVAR, the mass continuity equation is imposed as a weak constraint. This constraint builds up the relationship between different wind components. Gao et al (1999; 2004) found that this constraint is very effective in producing reasonable analyses of vertical velocity. When a stretching gird strategy is used in vertical direction, a special treatment (Hu et al. 2006a, 2006b), which assigns different weighting coefficients in horizontal and vertical direction, is needed to apply this constraint.

In our recent development, the modified ARPS model equations are also included as weak constraints in the 3DVAR scheme. These newly introduced constraints couple the wind components with the thermodynamic variables (Ge et al. 2007). In this study, for simplicity, only the mass continuity constraint is included because our focus is to disclose the relative importance of radial wind and reflectivity on storm-scale data assimilation. The cloud analysis was developed based on the Local Analysis and Prediction system (LAPS, Albers et al. 1996) with significant modifications by Zhang (1999), Brewster (2002), and Hu et al (2006a). The purpose of including the cloud analysis is to decrease the "spin up" time of storm development in numerical models.

3. Data assimilation experiments with simulated data

In this section, we evaluate the impacts of reflectivity and radial wind on radar data assimilation using simulated data. Such simulation experiments

are usually referred as observing system simulation experiments (OSSEs). The ARPS model is used in a 3D cloud model mode whereby the storm environment is horizontally homogeneous. The 20 May 1977 Del City, Oklahoma tornadic supercell storm is used to conduct several series of experiments. This storm has been thoroughly studied by multiple Doppler analysis and numerical simulation (Ray at al. 1981; Klemp et al. 1981; and Klemp and Rotunno 1983).

The model is configured using 67 × 67 × 35 grid points and 1km × 1km × 0.5km grid intervals in the x,y,z directions respectively, so as to create a physical domain of 64 × 64 × 16 km. The simulation starts with a modified sounding (as in Klemp et al, 1981) which favors the development of supercell thunderstorms. A thermal bubble of 4K perturbation is used to initiate a storm, and this bubble is centered at x=48 km, y=16 km and z=1.5 km with the lower-left corner of the domain as the origin. The radius of the bubble is 10 km in x and y directions and 1.5 km in the z direction. The three-category ice microphysical scheme of Lin et al. (1983) is used together with a 1.5-order turbulent kinetic energy subgrid parameterization. Open boundary conditions are used for the lateral boundaries and rigid wall conditions for the top and bottom boundaries. An upper-level Rayleigh damping layer is also included to reduce wave reflection from the top of the model.

The simulation runs for 90 min. To keep the right-moving storm near the center of the model domain, a mean storm speed (U=3 ms^{-1}, V=14 ms^{-1}) is subtracted from the sounding. Fig.1a-d shows horizontal cross sections of simulated wind vectors, contours of reflectivity and potential temperature (shaded) at surface and Fig. 2a-d shows horizontal cross sections of simulated wind and contours of vertical velocity at 3 km above ground level from 30 min to 90 min of model integration time respectively. The initial convective cell strengthens over the first 30 min and begins to split into two cells around 50 min. At about 90 min into the simulation, the right mover is near the center of the domain as expected and the left mover located at the northwest corner. (Fig. 1 a-d). A strong rotating updraft associated with the right-moving storm (about 22 m s^{-1}) is evident at 50 min, and moves slowly to southeast and remains the same strength at 90 min (Fig 2a-d). The evolution of the simulated storm is qualitatively similar to that described by Klemp and Wilhelmson (1981).

Two pseudo radars are placed at south of the analysis domain at (X=0 km, Y=0 km, Z=0 km) and (X=64 km, Y=0 km, Z=0 km). Simulated radar observations including both radial wind and reflectivity from two pseudo Doppler radars are obtained at model grid points by sampling the evolution of this simulated storm every 5 min from 30 min to 90 min. The elapsed times for the volume scans of two radars are neglected, and thus we assume that the radial wind observations are simultaneous. For simplicity, the two radars will cover all horizontal physical grids (i.e. 64 × 64) which assumes that the radars sweep

almost continuously in horizontal direction. The elevation angles are chosen to reproduce the scanning strategy of the VCP 11 mode for the WSR-88D network. The simulated radar data are only specified in precipitation regions (where reflectivity is greater than zero). To simulate the radar's statistical error, a 1m s^{-1} random error is added to the radial velocities in the pseudo observation dataset.

Three intermittent data assimilation experiments are performed with an interval of 5 min and a window covering t=30 min to t=90 min of the model simulation. In the first experiment, only radial velocity data are assimilated using ARPS 3DVAR, and this experiment is referred as SiVrOnly. In the second experiment, only reflectivity data are assimilated using the cloud analysis scheme, so it is named as SiRfOnly. In this cloud analysis scheme, the mixing ratio of precipitation (including rain water, snow, and hail) and potential temperature are adjusted within the cloud analysis based on reflectivity measurements. The other hydrometeor variables are not adjusted to avoid negative impacts on the balance of model equations when rapid analysis cycles are applied. In the third experiment, both radial velocity and reflectivity data are used, and it is named SiVr&Rf. These three experiments are designed to survey the relative impacts of different data types on radar data assimilation over a given data assimilation window. There are 13 assimilation cycles with 5 min interval in these 3 experiments. The ARPS 3DVAR system is used to first create the model initial condition and then the ARPS system runs for a 5-min forecast starting from this initial analysis. This intermittent assimilation cycle is applied every 5 min until the end of assimilation period.

To investigate which type of data has more impact on intermittent data assimilation cycles, we estimate how the model variables, such as wind components, potential temperature, moisture are retrieved. Fig. 1 shows the horizontal winds, perturbation potential temperature and reflectivity at 250 m AGL (first model level above surface) and Fig. 2 shows the horizontal wind, and vertical velocity fields at 3.5 km AGL, at 30, 50, 70 and 90 min of model time. They are shown for the truth simulation, cycled 3DVAR assimilation for experiments SiVrOnly, SiRfOnly and SiVr&Rf, as described above. For the SiVrOnly experiment, Fig. 1e shows that analyzed horizontal wind field has a small convergence area near the center of model domain at the first cycle of assimilation, but the reflectivity field is zero because reflectivity is not assimilated. Fig. 1i shows quite opposite results to Fig. 1e, with no wind perturbation, but the reflectivity field is quite similar to the truth run (Fig. 1i, vs Fig. 1a). In SiVr&Rf, both radial velocity and reflectivity are used and the analysis established the pattern of precipitation and the storm structure quite well. At the 3.5 km level, an updraft is produced at the correct location for both SiVrOnly and SiVr&Rf experiments (Fig. 2e, m), but there is no updraft for SiRfOnly, as expected. After four more analysis cycles at t = 50 min, the low-level flow immediately

underneath the storm cells becomes closer to the truth (Fig. 1f, g, n vs 1b), but the cold pool and reflectivity areas are still smaller for experiment SiVrOnly. At the 3.5 km level, the perturbation horizontal winds and the updrafts are well captured in SiVrOnly and SiVr&Rf experiments, and the strength of the updraft for the SiRfOnly is good, but the pattern is somewhat different from the truth (Fig. j vs 2b).

By t = 70 min, the analysis is further improved. By this time, there is no significant difference from the truth in either the low-level and mid-level fields (Fig. 1g, k, o and Fig. 2g, k, o). The cold pool in experiment SiVrOnly looks closer to the truth than other two experiments, but the reflectivity field is little bit weaker than other two experiments and the truth. In mid-levels (Fig 2k), the retrieved mesocyclone is present for experiment SiRfOnly, but its pattern is quite different from truth; this behavior becomes worse for the final assimilation cycle (Fig 2l). General storm structures including the precipitation pattern are well retrieved at the final assimilation cycle in all three experiments though the results from SiRfOnly are worse than the other two, especially for the wind pattern. From analyzing these individual model generated fileds, we can see that both radial wind and reflectivity have positive impacts on radar data assimilation for retrieving model variables which are not directly observed by two radars. Radial velocity mainly benefits the retrieval of model's dynamic variables, while reflectivity mainly benefits the establishment of model's precipitation pattern.

Although the root-mean-square (rms) error is not a good verification tool for storm scale phenomena, we still use it here for quantitative comparison among different experiments. The RMS errors for several analyzed model variables, V_h, w, θ', and q_v are shown in Table 1. It is clear the rms errors for experiment SiVrOnly decrease with time rapidly. In contrast, the rms errors of selected model variables for SiRfOnly experiment increase with time, especially for both horizontal and vertical wind components. This indicates that assimilating reflectivity data actually introduces error during the assimilation cycles, though these data also can assist in building up storm cells during the assimilation cycles. For experiment SiVr&Rf, the rms errors for θ' increases with time, but not as much as when assimilating the reflectivity only, and errors for V_h, w, and q_v decrease with time gradually. This indicates that assimilating both radial velocity and reflectivity data has mixed results in term of rms errors and introduces less error to the model than when assimilating reflectivity only.

Tabel 1. The RMSE of horizontal wind(V_h), vertical velocity(w), potential temperature(θ), water vapor mixing ratio (qv)

Exps	Vars	0 min	20 min	40 min	60 min
SiVrOnly	V_h	2.65	2.15	1.98	1.93
	w	2.89	2.67	1.98	1.79
	θ	2.25	1.92	1.73	1.60
	qv	0.78	0.42	0.43	0.34
SiRfOnly	V_h	5.62	6.29	7.77	9.68
	w	4.95	7.00	6.19	6.85
	θ	2.25	3.08	3.47	4.07
	qv	0.78	0.81	0.84	0.78
SiVr&Rf	V_h	2.65	2.27	2.36	2.40
	w	2.89	3.14	2.49	2.52
	θ	2.25	2.94	4.17	5.34
	qv	0.78	0.53	0.58	0.57

To conclude, it is shown that assimilating radial velocity only (SiVrOnly) produces the best results at the final assimilation step, but it needs time to spin up the storm. Assimilating reflectivity data helps to reduce the spin-up time, but it also introduces some additional error. There are two possible sources for this additional error: one is that the cloud analysis package, which is used to assimilate reflectivity data and is based on empirical laws, has lots of sensitive parameters to be tuned and obtaining an optimal parameter setting is difficult. Another is that the nonlinear interaction between model variables (especially between dynamic variables and hydrometeor related variables) is not well handled in the current ARPS 3DVAR system and a dynamically consistent analysis is not reached due to the lack of suitable equation constraints.

4. Experiment with May 7 Greensburg tornadic storm case

In this section, we investigate the impacts of reflectivity and radial wind on radar data assimilation with a real data case – the 4-5 May 2007 Greensburg tornadic thunderstorm case. This case is chosen because it is well documented and produced one of the strongest tornadoes in recent years. The storm complex produced 18 tornadoes in the Dodge City forecast area and 47 tornado reports in Kansas, Nebraska and Missouri. The tornado started moving through Greensburg at 0245 UTC 5 May 2007 (21:45 CDT 4 May) and destroyed over 90 % of the town. The tornado damage was rated at EF5 - the highest rating on the Enhanced Fujita scale (McCarthy et al., 2007).

The synoptic setting for this event at 0000 UTC 5 May consisted of a deep trough over the western United States with an upper-level short-wave trough starting to move over western Kansas (Fig. 3a). A surface low was present over southeastern Colorado, and a quasi-stationary front extended from the low across northwest Kansas and into northeast Nebraska (Fig. 3b). A dryline stretched generally southward across western Kansas, Oklahoma, and into west Texas. A very moist and unstable air mass was found east of the dryline, where values of surface-based convective available potential energy (CAPE) were above 4000 J kg^{-1} across central Oklahoma and southcentral Kansas. Values of 0-3 km storm-relative environmental helicity (SREH) were in excess of 150 $m^2 s^{-2}$ throughout much of Oklahoma and Kansas, providing an environment favorable for supercell thunderstorms.

Initial storm development occurred over the northern Texas panhandle/Oklahoma border around 2210 UTC on 4 May 2007. A complex cell evolution ensued in which several storm splits were observed in succession over the next 2 h. As one of the storms crossed the border into Kansas near 0040 UTC, it split with the right-moving storm evolving into the tornadic supercell thunderstorm that passed over Greensburg. This storm moved from 212°(the direction with the north as 0° and clockwise turn, hereafter) at 13 ms^{-1} and developed its hook echo

signature by 0106 UTC. Between 0130 UTC and 0148 UTC, a strong middle-level mesocyclone was very clear and persistent in the data of Dodge City WSR-88D radar (not shown). The supercell was observed to take on a classic hook echo shape by 0230 UTC as the strength of its rotation increased dramatically. The tornado that eventually produced the violent EF-5 damage at Greensburg was first observed near 0200 UTC (Lemon and Umscheid 2007). Forecasters at the National Weather Service Dodge City Weather Forecast Office issued a tornado warning with 30 minutes lead-time for this event.

Over the next hour from 0230 to 0330 UTC, this tornadic supercell thunderstorm (which we call the dominant storm) turned a bit more to the right, moving from 219° as the storm motion slowly decreased from 10 m s^{-1} to near 8 m s^{-1} (Fig. 3, Lemon and Umscheid 2007). In comparison, the group of non-supercell thunderstorms to the northwest of the dominant storm moved much faster at 23 m s^{-1} from 206°. While the violent EF-5 tornado that hit Greensburg dissipated near 0305 UTC, a second strong EF-3 tornado developed near 0303 UTC, lasted for 65 min, and had a path length of over 43 km. This 1-h period from 0230 to 0330 UTC is selected for study since this dominant thunderstorm has classic supercell characteristics, including a well-defined mesocyclone and hook echo, during this time period (Fig. 3). In addition, the storm motion is fairly steady and strong tornadoes are observed throughout the period. Thus, this 1-h period is very good for testing a convective-scale forecast system.

For this real data case experiment, we use 3-km grid spacing with 200x200 grid points in the horizontal. The domain is selected with sufficient coverage to contain the principal features of interest while maintaining some distance between primary storms and the lateral boundaries. The model uses 47 terrain-following vertical layers, with nonlinear stretching, via a hyperbolic tangent function, that yields a spacing of 100 m at the ground that expands to approximately 800 m at the top of the domain. Similar to idealized case, the ARPS 3DVAR technique is used to create rapid analysis cycles and the cloud analysis scheme follows the 3DVAR analysis step to assimilate the radar reflectivity data. In addition, the mixing ratio of precipitation (including rain water, snow, and hail) and potential temperature are adjusted within the cloud analysis based on reflectivity measurements, and the other hydrometeor variables are not adjusted to avoid negative impacts of these adjustments on the balance of model equations.

For this real data case, we again focus on understanding the impacts of radial velocity and reflectivity on numerical forecast. In the first analysis and forecast experiment (named experiment ReVrOnly), only radial velocity observations are used. For the second experiment (named ReRfOnly), only reflectivity observations are used. Both radial velocity and reflectivity data are used in the third experiment (named ReVr&Rf). These three experiments allow us to assess the relative importance of radial velocity

and reflectivity data.

For all the experiments, radar data from six radars at Dodge City (KDDC), (Vance AFB, OK (KVNX), Wichita Kansas (KICT), Oklahoma City (KTLX), Amarillo TX (KAMA) and Topeka Kansas (KTWX) are used in the 3DVAR and cloud analysis system. Each experiment consists of a 1-h assimilation period (from 0130-0230 UTC) and a 1-h forecast period (0230-0330 UTC). The background and boundary condition come from an analysis from a mesoscale ensemble assimilation system (Stensrud and Gao, 2009). While Stensrud and Gao (2009) performed a 3DVAR analysis only at one time level before the forecast is launched, the present study uses an assimilation period that consists of thirteen analysis cycles at 5-min intervals, where a 5 min ARPS forecast follows each analysis until the end of the 1-h assimilation period. From the final analysis, a 1-h forecast is launched.

For all three experiments, we use analyses from WSR-88D data for verification. The evolution of the storm as indicated by the analyzed radar reflectivity, horizontal winds, and vertical vorticity at the 2 km MSL is shown in Fig. 4 from 0230 to 0330 UTC. The development of hook feature for the major supercell near Greensburg area around 0240 UTC is very clear. The wind analysis at this level indicates a very strong mid-level cyclonic circulation. This storm moved gradually in the northeast direction (Fig 4). During this period, the dominant storm cell produced the most intense tornado that hit the town of Greensburg. The storm maintained a very strong circulation and continued to move to the northeast, and second tornado developed coincident with the end of Greensburg tornado just northeast of the town (McCarthy 2007).

Our first analysis and forecast experiment (ReVrOnly) that uses the radial velocity observations only is able to capture the path of the storm that produced the Greensburg tornado during 1-h period of forecast (Fig 5). However, the initial storm produced at the end of 1-h intermittent assimilation (from 0130-0230 UTC) is generally very weak (Fig 5a). There are two reasons for this result. The first is that no reflectivity is assimilated, so the storm has to be "spin up" by itself through the internal storm dynamics based upon only radial wind observations. The second reason is that during the 1-h assimilation period the observed dominant storm is located in between several nearby radars (KDDC, KVNX, KICT), but none of the radars is very close to the storm. Thus, only the mid-level storm signatures are observed, and so the storm develops from the middle levels. At the end of 1-h intermittent assimilation (0230 UTC), the precipitation is still under development and has not reached to the ground yet. However, the location of the storm and its dynamics are well established, and so the forecast storm quickly develops its hook echo signature during the first 10 min (Fig 5b) and maintains a strong circulation throughout the 1-h forecast. The circulation appears very strong during 0240-0250 UTC period during

which time the the strong tornado hit Greensburg. However, because no reflectivity data are assimilated, the area of precipitation is relatively small compared to the analysis (Fig 4).

In the second experiment (ReRfOnly), only reflectivity observations are used. The analyzed reflectivity pattern after 1-h of intermittent assimilation looks reasonable (Fig 6a). But the wind vectors, especially near and in the storm, are very different from the 3DVAR analysis (Fig 4a). This indicates that the storm dynamic structure is not fully captured during the 1-h assimilation of reflectivity using the cloud analysis scheme. While the purpose of using the cloud analysis is to reduce the spin-up period for forecasts beginning from a single analysis, the repeated application of the cloud analysis in the high-frequency assimilation cycles may lead to unrealistically high values for hydrometer related variables, such as rain water mixing ratio, snow mixing ratio, even potential temperature. To reduce this unrealistic effect, it is important to adjust model dynamic variables by assimilating radial wind observations simultaneously, which will be discussed later (also see idealized case). As indicated by the forecast in Fig. 6, the initially dominant cell on the right (south side) propagates much faster to the northeast than the observed storm and eventually merges with some smaller cells (Fig. 6c, d, e). By the end of the one hour forecast period, the merged cell has grown into a large storm complex and is located too far northeast compared to the analysis (Fig. 6f) and the observation (Fig. 4f). There is no obvious circulation associated with tornadic signature of the thunderstorm. While a weak circulation exists in Fig 6c, d, the location is not correct. In general, the results from this set of experiments are not very encouraging.

The third experiment (ReVr&Rf) yields the best results, as the evolution of the forecast storm is closest to the analysis. Fig. 7a shows that both the reflectivity and wind field look reasonable compared to the analysis (Fig 4a), and there is a very small positive vorticity center at 2-km MSL. The 10-min forecast valid at 0240 UTC indicates a weak hook echo near Greensburg accompanied by a stronger mesocyclone than that of Fig. 7a. The storm moves slowly to the northeast, develops a strong hook echo, and maintains its strength throughout the entire one-hour forecast period. The whole 1-h forecast of the dominant cell that produced the Greensburg tornado compares reasonably well with the analyses in terms of the structure, location and evolution of the convective storm. Several small cells that are separate from the dominant storm also propagate to the northeast and become weaker and weaker until some finally disappear. This does not completely agree with the analysis, but is not the main concern of forecasters on this day. These results indicate that using both radial velocity and reflectivity data in the 3DVAR assimilation system is more beneficial to producing a reasonable forecast of this severe tornadic thunderstorm event than using these two

data types separately.

5. Summary and Conclusion

The WSR-88D network allows meteorologists to track severe weather events and provide better warning information to the public, ultimately saving lives and reducing property damage. However, the assimilation of such data into NWP models to provide physically consistent three-dimensional analyses and short-term forecasts has not been extensively explored. Doppler radar is the only operational instrument capable of providing in-storm observations of sufficient spatial and temporal resolution to capture convective-scale phenomena. Therefore, the effective assimilation of Doppler radar data into operational convection-resolving models is of increasing importance in our quest to extend warning lead times (Stensrud et al. 2009). Among the existing data assimilation methods, the 3DVAR system is a very computationally efficient method that can use radar data in real-time mode and in very high resolution both spatially and temporally. In this study, the impact of assimilating radial velocity and reflectivity data from a WSR-88D network near central Oklahoma is examined using both an idealized and a real data case. The ARPS 3DVAR, combined with a complex cloud analysis package, is used to produce analyses in high-frequency intermittent assimilation cycles. The ARPS model is used to do the 1-hour long numerical forecast for the real data case. Our purpose is to examine the relative importance of assimilating radial velocity and reflectivity data on storm-scale data assimilation and forecasting for very strong convective weather events.

For the idealized case, a set of experiments that differ in the type of data used are performed to identify the impact of radial velocity and reflectivity data when using two pseudo WSR-88D radars. It is found that by assimilating radial velocity data only, the model can predict the timing and evolution of a simulated supercell thunderstorm with great accuracy. In contrast, large errors emerge when only reflectivity data are assimilated. These errors are produced during the updating of hydrometer-related variables and the temperature adjustment that occurs in the cloud analysis package. When both radial velocity and reflectivity are used, the analysis has less error than seen when assimilating reflectivity only, but has more error than seen when only radial velocity is assimilated. However, assimilating reflectivity data can reduce a storm's "spin up" time significantly. Thus, to obtain the maximum benefit from radar data, both radial velocity and reflectivity should be assimilated in the most appropriate way.

For the observed Greensburg tornadic thunderstorm case of 4-5 May 2007, three experiments are undertaken that are very similar to those from idealized data case. It is found that by assimilating only radial velocity data the model can reproduce the supercell thunderstorm that produced Greensburg tornado very well. In contrast, by

assimilating only reflectivity data, the model fails to reproduce the Greensbeurg supercell thunderstorm. However, when both radial velocity and reflectivity data are assimilated, the dominant storm cell that produced the Greensburg tornado is reproduced most accurately in term of the structure, location and evolution of storm. These results suggest that the assimilation of radial velocity data is essential for the prediction of supercell thunderstorms, likely due to their helical updrafts that play such an important dynamic role in storm development and evolution. Though reflectivity data is fundamental to storm tracking and quantitative precipitation estimation (QPE) and the assimilation of such data into NWP models can reduce the model spin-up time, it may be not as important as radial velocity. This is due to reflectivity being related to more inactive model variables and a lot of uncertainties in model microphysics further complicates its usage in storm scale NWP. However, the inclusion of reflectivity data with radial velocity data yields the best results, and for weaker thunderstorms reflectivity data may be very important. More research is needed to confirm these conclusions.

Acknowledgement: This work was primarily supported by NSF grant ATM-073870 and the National Severe Storm Laboratory under grant number NSSL/NOAA-085010. The first and last authors also acknowledge the support by NSF EEC-0313747, and ATM-0802888.

References

Albers, S. C., J. A. McGinley, D. A. Birkenheuer, and J. R. Smart, 1996: The local analysis and prediction system (LAPS): Analysis of clouds, precipitation and temperature. *Wea. Forecasting*, **11,** 273-287.

Brewster, K., 1996: Application of a Bratseth analysis scheme including Doppler radar data. *Preprints, 15th Conf. Wea. Anal. Forecasting*, Norfolk, VA, Amer. Meteor. Soc., 92-95.

Brewster, K., 2002: Recent advances in the diabatic initialization of a non-hydrostatic numerical model. *Preprints, 15th Conf on Numerical Weather Prediction and 21st Conf on Severe Local Storms*, San Antonio, TX, Amer. Meteor. Soc., J6.3.

Brewster, K., M. Hu, M. Xue, and J. Gao, 2005: Efficient assimilation of radar data at high resolution for short-range numerical weather prediction. *WWRP International Symposium on Nowcasting and Very Short range Forecasting*, CDROM 3.06.

Brotzge, J., K. Brewster, V. Chandrasekar, B. Philips, S. Hill, K. Hondl, B. Johnson, E. Lyons, D. McLaughlin, and D. Westbrook, 2007: CASA IP1: Network operations and initial data. *23rd International Conf. on Interactive Information Processing Systems (IIPS) for Meteor., Ocean., and Hydrology*, AMS Conf.

Caya, A., J. Sun, and C. Snyder, 2005: A comparison between the 4D-VAR and the ensemble Kalman

filter techniques for radar data assimilation. *Mon. Wea. Rev.*, **133,** 3081–3094.

Dowell, D.C., F. Zhang, L.J. Wicker, C. Snyder, and N.A. Crook, 2004: Wind and Temperature Retrievals in the 17 May 1981 Arcadia, Oklahoma, Supercell: Ensemble Kalman Filter Experiments. *Mon. Wea. Rev.*, **132**, 1982–2005.

Droegemeier, K. K., 1990: Toward a science of storm-scale prediction. *Preprint, 16th conf. on Severe Local Storms*, Kananaskis Park, Alberta, Canada, Amer. Meteor. Soc., 256-262.

Droegemeier, K. K., 1997: The numerical prediction of thunderstorms: Challenges, potential benefits, and results from real time operational tests. *WMO Bulletin*, **46,** 324-336.

Evensen, G., 1994: Sequential data assimilation with a nonlinear quasi-geostrophic model using Monte Carlo methods to forecast error statistics. *J. Geophys. Res.*, **99,** 10143-10162.

Gao, J., M. Xue, A. Shapiro and K. K. Droegemeier, 1999: A Variational Method for the Analysis of Three-Dimensional Wind Fields from Two Doppler Radars. *Mon. Wea. Rev.*, 127, 2128–2142.

Gao, J., M. Xue, K. Brewster, F. Carr, and K. K. Droegemeier, 2002: New development of a 3DVAR system for a nonhydrostatic NWP model. *Preprint, 15th Conf. Num. Wea. Pred. and 19th Conf. Wea. Anal. Forecasting*, San Antonio, TX, Amer. Meteor. Soc., 339-341.

Gao, J., M. Xue, K. Brewster, and K. K. Droegemeier, 2004: A three-dimensional variational data analysis method with recursive filter for Doppler radars. *J. Atmos. Ocean. Tech.*, **21,** 457-469.

Gao, J. and M. Xue, 2008: An efficient dual-resolution approach for ensemble data assimilation and tests with assimilated Doppler radar data. *Mon. Wea. Rev.* **136**, 945-963.

Ge, G. and J. Gao, 2007: Latest development of 3DVAR system for ARPS and its application to a tornadic supercell storm. *22nd Conf. on Weather Analysis and Forecasting/18th Conf. on Numerical Weather Prediction*, Park City, Utah, Amer. Meteor. Soc., 2B.6

Ge, G., J. Gao, K. Brewster, and M. Xue,, 2009: Impacts of Beam Broadening and Earth Curvature on 3D Variational Radar Data Assimilation with Two Doppler Radars, *J. Tech.*, (Submitted).

Hu, M., M. Xue, and K. Brewster, 2006a: 3DVAR and cloud analysis with WSR-88D level-II data for the prediction of Fort Worth tornadic thunderstorms. Part I: Cloud analysis and its impact. *Mon. Wea. Rev.*, **134,** 675-698.

Hu, M., M. Xue, J. Gao, and K. Brewster, 2006b: 3DVAR and cloud analysis with WSR-88D level-II data for the prediction of Fort Worth tornadic thunderstorms. Part II: Impact of radial velocity analysis via 3DVAR. *Mon. Wea. Rev.*, **134,** 699-721.

Lin, Y., R. D. Farley and H. D. Orville, 1983: Bulk Parameterization of the Snow Field in a Cloud Model. *Journal of Applied Meteorology*, 22, 1065-1092.

Klemp, J. B. and R. B. Wilhelmson, 1978: Simulations of right- and left-moving storms produced through storm splitting. *J. Atmos. Sci.*, 35, 1097-1110.

Klemp, J. B. and R. Rotunno, 1983: A study of the tornadic region within a supercell thunderstorm. *J. Atmos. Sci.,* 40, 359-377

Klemp, J. B., R. B. Wilhelmson and P.S. Ray, 1981: Observed and numerically simulated structure of a mature supercell thunderstorm. J. Atmos. Sci., 38, 1558-1580.

Purser, R. J., W.-S. Wu, D. Parrish, and N. M. Roberts, 2003a: Numerical aspects of the application of recursive filters to variational statistical analysis. Part I: Spatially homogeneous and isotropic Gaussian covariances. *Mon. Wea. Rev.,* **131,** 1524–1535.

——, ——, ——, and ——, 2003b: Numerical aspects of the application of recursive filters to variational statistical analysis. Part II: Spatially inhomogeneous and anisotropic general covariances. *Mon. Wea. Rev.,* **131,** 1536–1548.

Ray., B. , C. Johnson, K. W. Johnson, J. S. Bradberry, J. J. Stephens, K. K. Wagner, R. B. Wilhelmson, and J.b .Klemp, 1981: The morphology of several tornadic storms on 20 May 1977. *J. Atmos. Sci.*, 38, 1643-1633.

Schenkman, A., M. Xue, A. Shapiro, K. Brewster, and J. Gao, 2009: Storm-scale data assimilation for the analysis and prediction of a tornadic convective system: The impact of high-resolution X-band radar data. Mon. Wea. Rev., Submitted.

Snyder, C. and F. Zhang, 2003: Assimilation of simulated Doppler radar observations with an ensemble Kalman filter. *Mon. Wea. Rev.*, **131,** 1663-1677.

Stensrud, D. J., M. Xue, L. Wicker, K. Kelleher, M. Foster, J. Schaefer, R. Schneider, S. Benjamin, J. Ferree, J. Tuell, and J. Hayes, 2009: Convective-scale Warn on Forecast: A Vision for 2020. *Bull. Am. Meteor. Soc.***,** (accepted).

Stensrud, D. J., and J. Gao, 2009: Importance of inhomogeneous environmental initial conditions to ensemble storm-scale radar data assimilation and very short range forecasts. *Mon. Wea. Rev.***,** (submitted).

Sun, J., D. W. Flicker, and D. K. Lilly, 1991: Recovery of three-dimensional wind and temperature fields from simulated single-Doppler radar data. *J. Atmos. Sci.*, **48,** 876-890.

Sun, J. and N. A. Crook, 1997: Dynamical and microphysical retrieval from Doppler radar observations using a cloud model and its adjoint. Part I: Model development and simulated data experiments. *J. Atmos. Sci.*, **54,** 1642-1661.

Sun, J. and N. A. Crook, 1998: Dynamical and Microphysical Retrieval from Doppler Radar Observations Using a Cloud Model and Its

Adjoint. Part II: Retrieval Experiments of an Observed Florida Convective Storm. *J. Atmos. Sci.*, **55,** 835-852.

Sun, J., 2005: Initialization and numerical forecasting of a supercell storm observed during STEPS. *Mon. Wea. Rev.*, **133,** 793-813.

Tong, M. and M. Xue, 2005: Ensemble Kalman filter assimilation of Doppler radar data with a compressible nonhydrostatic model: OSS Experiments. *Mon. Wea. Rev.*, **133,** 1789-1807.

Xiao, Q., Y. Kuo, J. Sun, W. Lee, E. Lim, Y. Guo, and D. M. Barker, 2005: Assimilation of Doppler Radar Observations with a Regional 3DVAR System: Impact of Doppler Velocities on Forecasts of a Heavy Rainfall Case. *Journal of Applied Meteorology and Climatology*, **44,** 768-788.

Xue, M., K. K. Droegemeier, and V. Wong, 2000: The Advanced Regional Prediction System (ARPS) - A multiscale nonhydrostatic atmospheric simulation and prediction tool. Part I: Model dynamics and verification. *Meteor. Atmos. Physics*, **75,** 161-193.

Xue, M., K. K. Droegemeier, V. Wong, A. Shapiro, K. Brewster, F. Carr, D. Weber, Y. Liu, and D. Wang, 2001: The Advanced Regional Prediction System (ARPS) - A multi-scale nonhydrostatic atmospheric simulation and prediction tool. Part II: Model physics and applications. *Meteor. Atmos. Phys.*, **76,** 143-166.

Xue, M., D.-H. Wang, J.-D. Gao, K. Brewster, and K. K. Droegemeier, 2003: The Advanced Regional Prediction System (ARPS), storm-scale numerical weather prediction and data assimilation. *Meteor. Atmos. Physics*, **82,** 139-170.

Xue, M., M. Tong, and K. K. Droegemeier, 2006: An OSSE framework based on the ensemble square-root Kalman filter for evaluating impact of data from radar networks on thunderstorm analysis and forecast. *J. Atmos. Ocean Tech.*, **23,** 46–66.

Xue, M., K. K. Droegemeier, and D. Weber, 2007: Numerical prediction of high-impact local weather: A driver for petascale computing. *Petascale Computing: Algorithms and Applications*, Taylor & Francis Group, LLC, 103-124.

Zhang, J., F. Carr, and K. Brewster, 1998: ADAS cloud analysis. *Preprints, 12th Conf. on Num. Wea. Pred.*, Phoenix, AZ., Amer. Met. Soc., 185-188.

Zhang, J., 1999: Moisture and Diabatic Initialization Based on Radar and Satellite Observation, School of Meteorology, University of Oklahoma, 194.

Zhang, F., C. Snyder, and J. Sun, 2004: Impacts of initial estimate and observations on the convective-scale data assimilation with an ensemble Kalman filter. *Mon. Wea. Rev.*, **132,** 1238-1253.

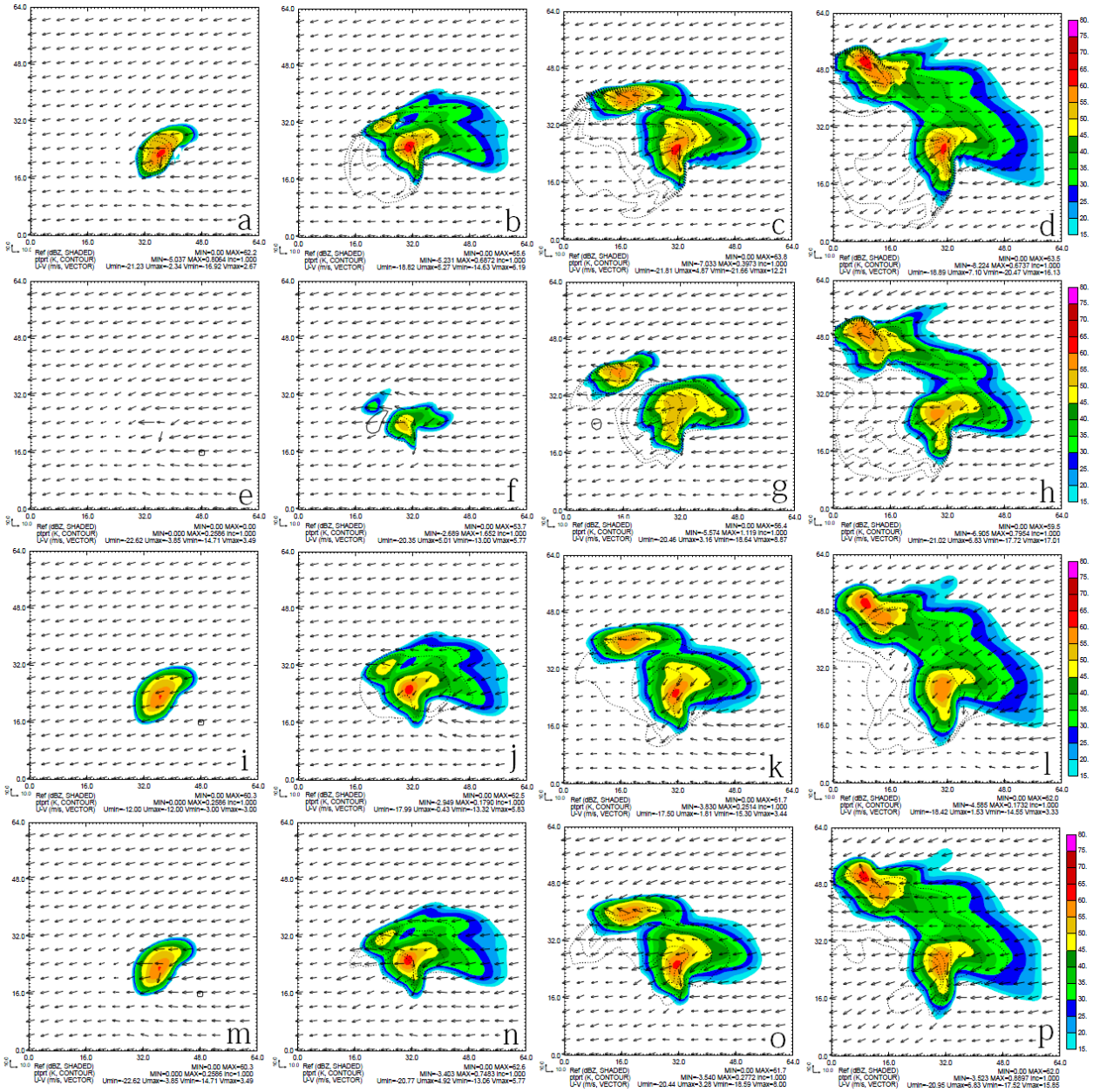

Fig. 1. The total u-v wind vector, perturbation potential temperature (contour at every 1K) and reflectivity (colored) at z=250m AGL and t=30min, 50min, 70min, and 90min respectively. (a), (b), (c), (d) are for truth simulation, (e), (f), (g), (h) are for Vr only experiment, (i), (j), (k), (l) are for Z only experiment, (m), (n), (o), (p) are for both Vr and Z experiment. Solid contour for positive, and dashed contour for negative.

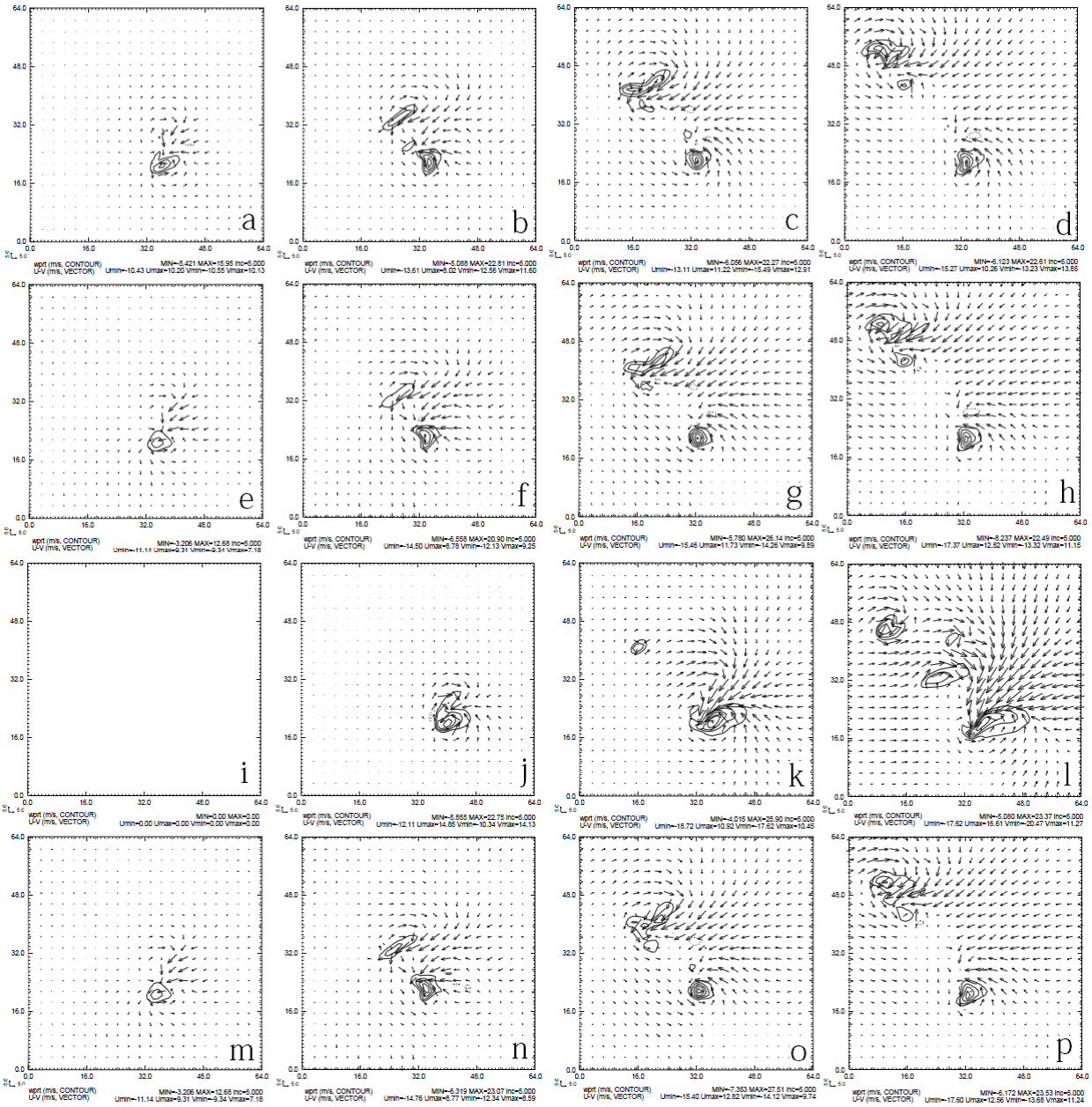

Fig. 2. The perturbation u-v wind vector, vertical velocity (contour at every 5m/s) at z=3.5km AGL and t=30min, 50min, 70min, and 90min respectively. (a), (b), (c), (d) are for truth simulation; (e), (f), (g), (h) are for Vr only experiment; (i), (j), (k), (l) are for Z only experiment; (m), (n), (o), (p) are for both Vr and Z experiment. Solid contour for positive, and dashed contour for negative.

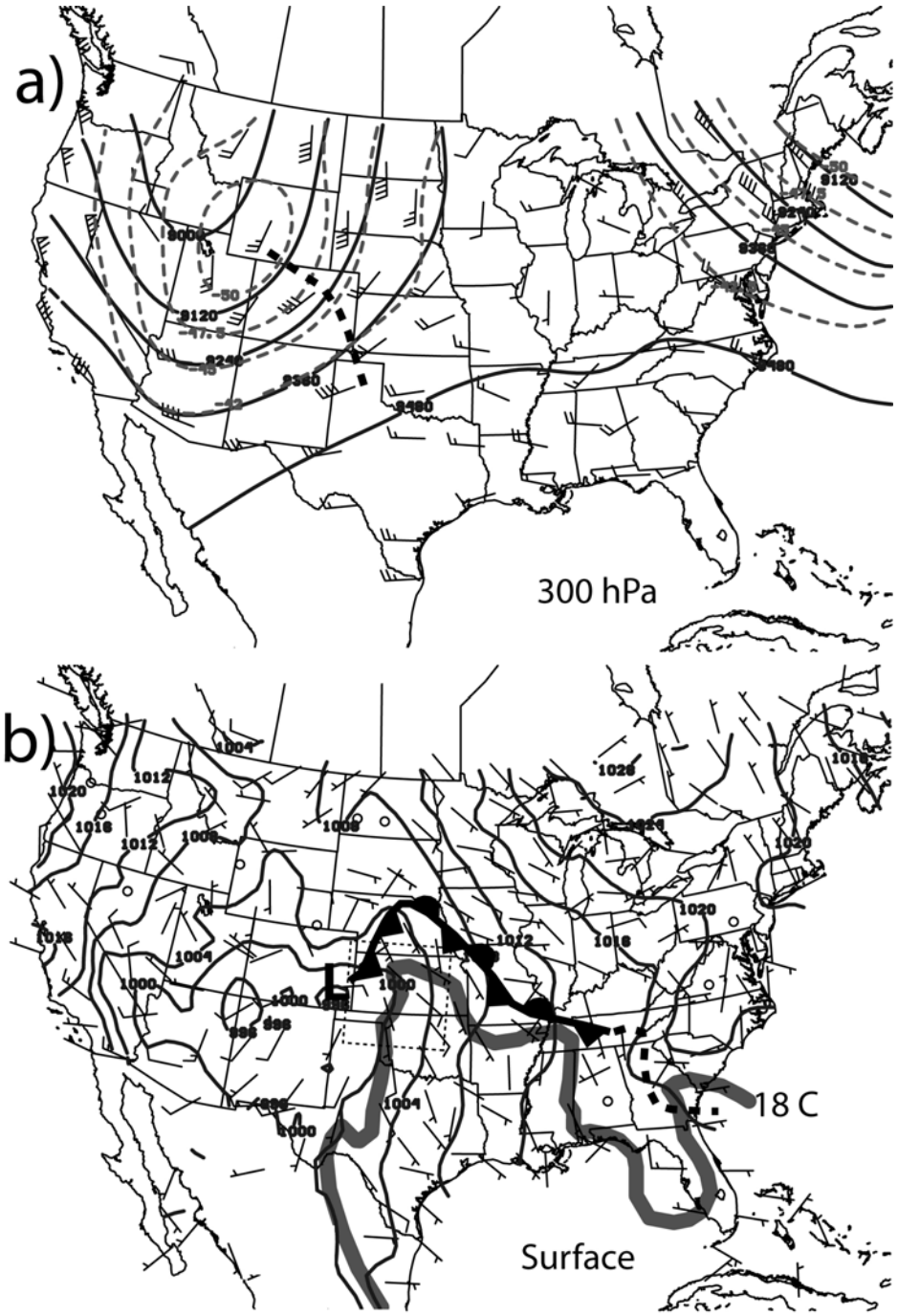

Fig. 3. Environmental conditions at 0000 UTC 5 May 2007 shown by (a) 300 hPa geopotential height (every 120 m), temperature (every 2.5 °C), and winds (full barb is 10 m s^{-1}), and (b) surface observations of mean-sea level pressure (every 4 hPa), winds (full barb is 10 m s^{-1}), and the 18°C dewpoint isoline.

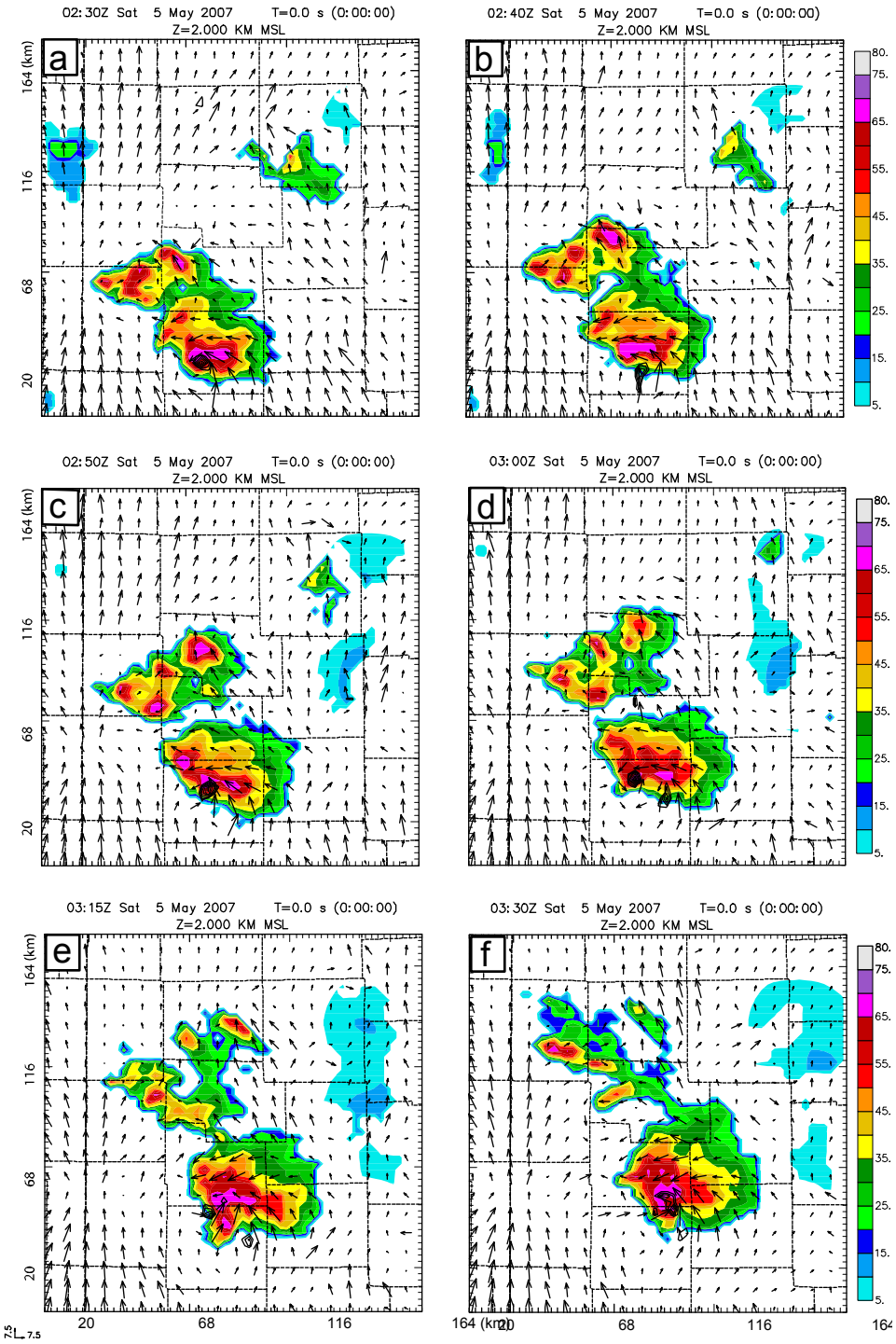

Fig. 4. Analyzed radar reflectivity (dBZ), horizontal winds, and vorticity at 2 km MSL using data from the KDDC, KICT, KVNX, KTLX, and KTWX Doppler radars valid at (a) 0230, (b) 0240, (c) 0250, (d) 0300, (e) 0315, and (f) 0330 UTC 5 May 2007 over western Kansas. Analyses created using the 3DVAR system.

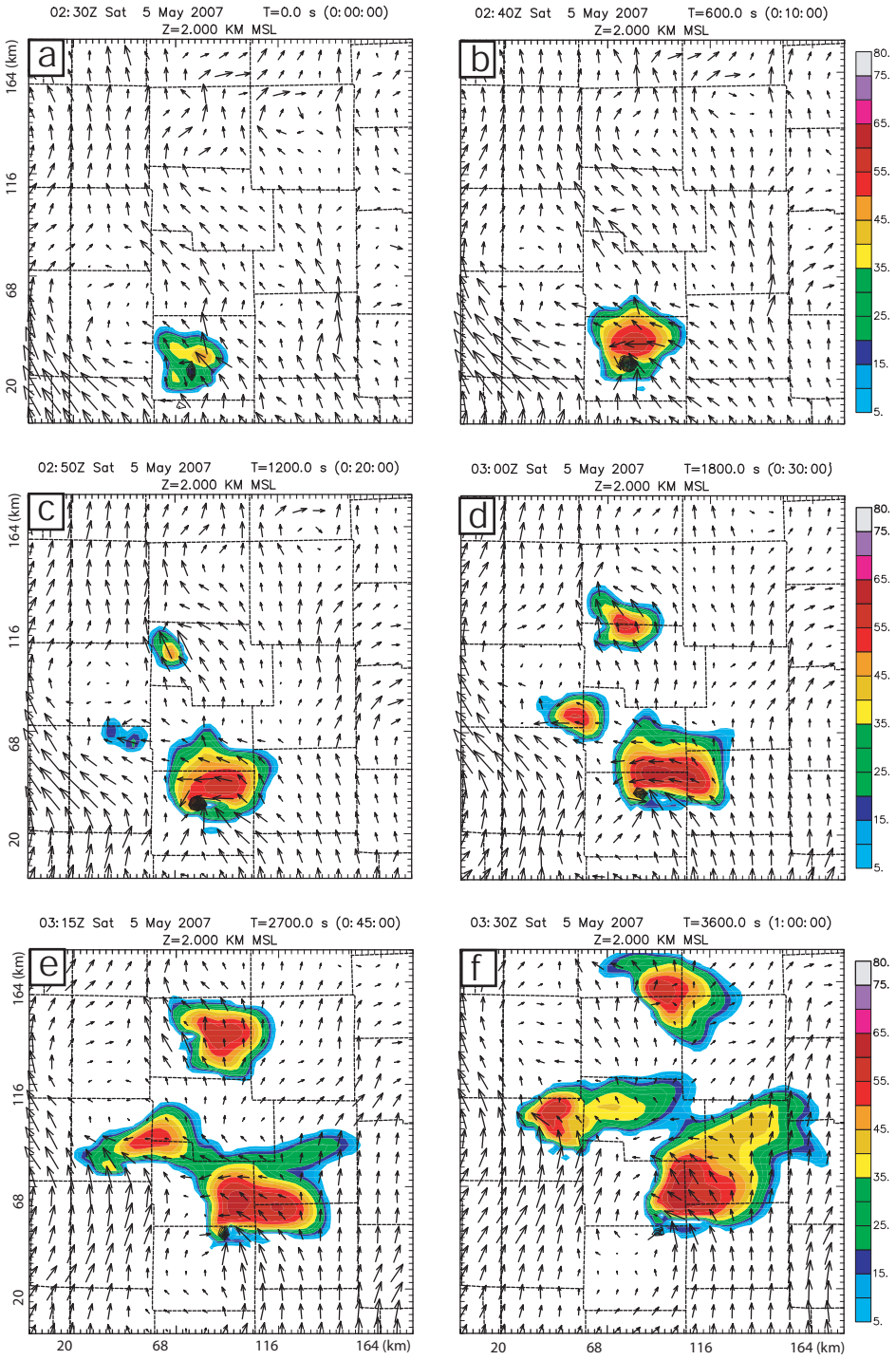

Fig. 5. As in Fig. 4, but for the forecast starting from the 3DVAR analysis at 0230 UTC 5 May 2007 for the Vr_only experiment.

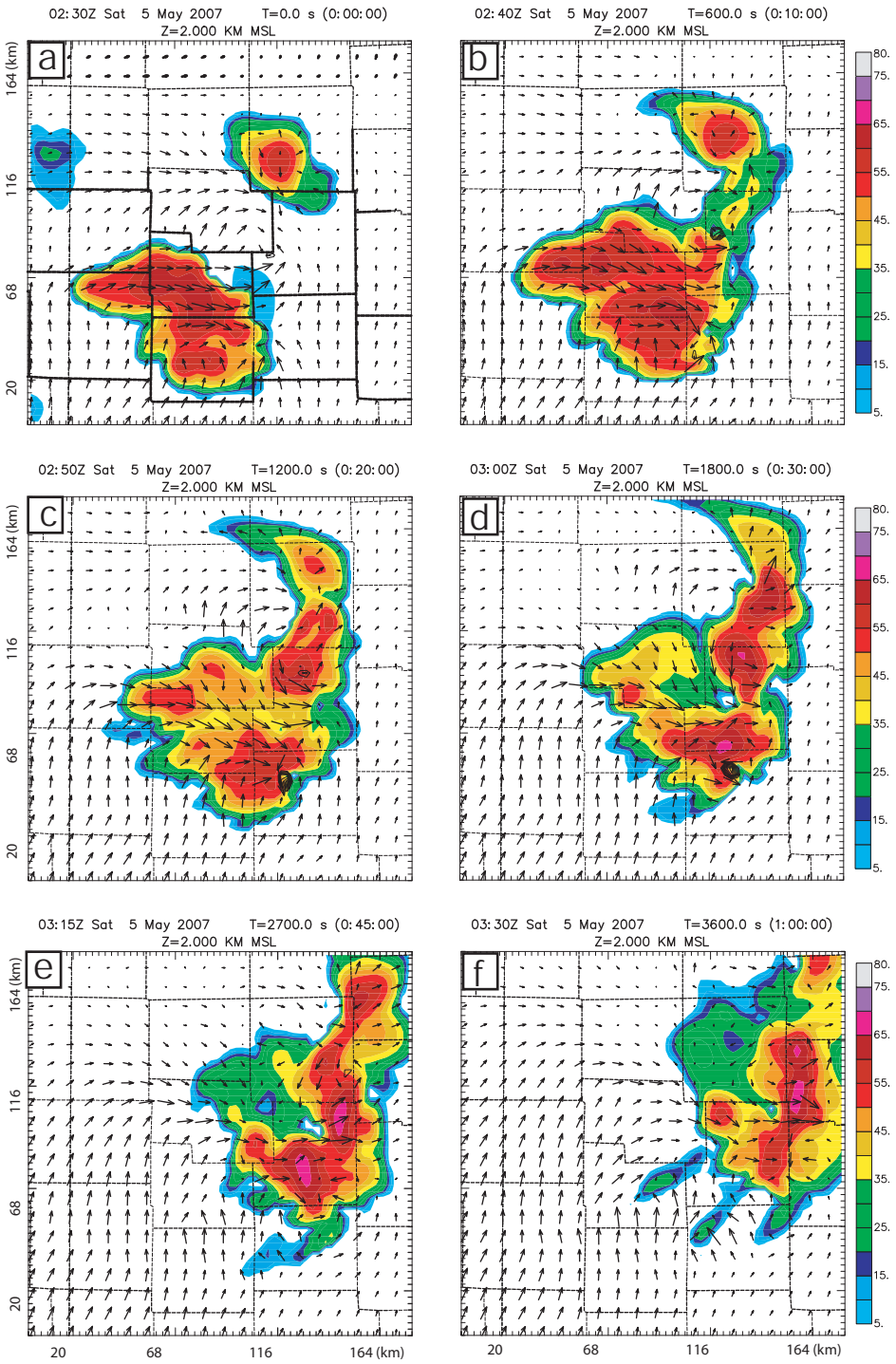

Fig. 6. As in Fig. 4, but for the forecast starting from the 3DVAR analysis at 0230 UTC 5 May 2007 for the Z_only experiment.

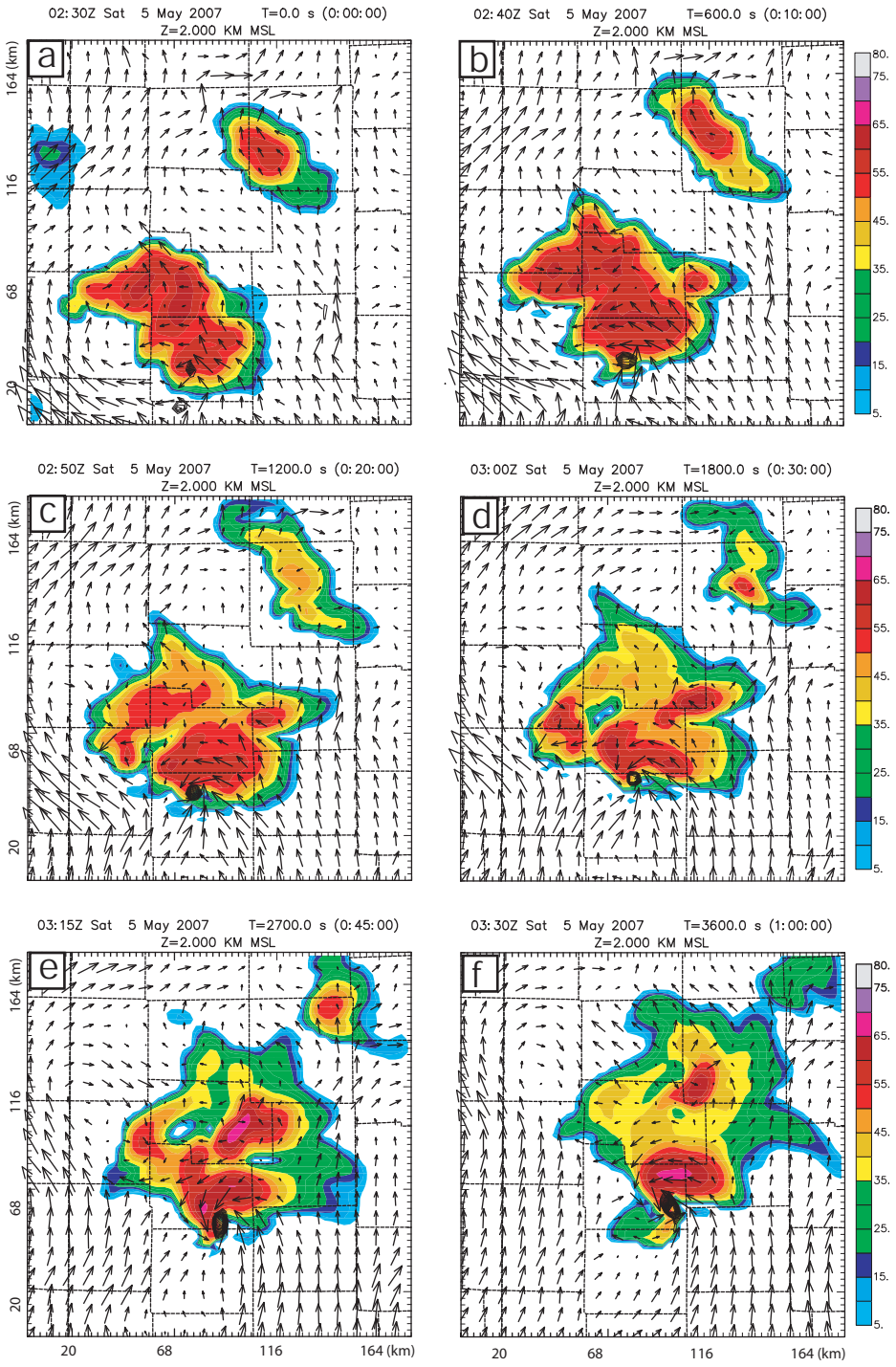

Fig. 7. As in Fig. 4, but for the forecast starting from the 3DVAR analysis at 0230 UTC 5 May 2007 for Vr_Z experiment.